Applied Ergonomics 82 (2020) 102963

Contents lists available at ScienceDirect

Applied Ergonomics

journal homepage: http://www.elsevier.com/locate/apergo

Prediction of coefficient of friction based on footwear outsole features

Arian Iraqi [a], Natasa S. Vidic [b], Mark S. Redfern [a], Kurt E. Beschorner [a,*]

[a] Department of Bioengineering, University of Pittsburgh, Benedum Engineering Hall #302, 3700 O'Hara St., Pittsburgh, PA, 15261, United States
[b] Department of Industrial Engineering, University of Pittsburgh, Benedum Engineering Hall #1025, 3700 O'Hara St., Pittsburgh, PA, 15261, United States

ARTICLE INFO

Keywords:
Slips
Coefficient of friction
Shoe safety
Shoe traction assessment
Slip-resistant

ABSTRACT

Traction testing of footwear is expensive, which may create barriers for certain users to assess footwear. This study aimed to develop a statistical model that predicts available coefficient of friction (ACOF) under boundary lubrication conditions based on inexpensive measurements of footwear outsole features. Geometric and material hardness parameters were measured from fifty-eight footwear designs labeled as slip-resistant. A robotic friction measurement device was used to quantify ACOF with canola oil as the contaminant. Stepwise regression methods were used to develop models based on the outsole parameters and floor type to predict ACOF. The predictive ability of the regression models was tested using the k-fold cross-validation method. Results indicated that 87% of ACOF variation was explained by three shoe outsole parameters (tread surface area, heel shape, hardness) and floor type. This approach may provide an assessment tool for safety practitioners to assess footwear traction and improve workers' safety.

1. Introduction

Falls on the same level have been ranked consistently among the top two disabling occupational injuries in the U.S. from 1998 to 2010 (Marucci-Wellman et al., 2015). In 2017, falls on the same level accounted for 16.2% (142,770 cases) of total non-fatal injuries in the private sector (U.S. Department of Labor- Bureau of Labor Statistics, 2018). Fatal injuries due to falls on the same level have increased from 111 cases in 2011 to 134 cases in 2016 (U.S. Department of Labor-Bureau of Labor Statistics, 2017). Direct workers' compensation costs due to falls on the same level have also grown from $4.2 billion in 1998 to $8.6 billion in 2010 (about $6.0 billion in 1998 dollars) (Marucci-Wellman et al., 2015). Slipperiness or slippery conditions are among the leading risk factors for occupational fall injuries (Courtney et al., 2001), and often occur due to exposure to liquid contamination (Bell et al., 2008). Footwear interventions tend to reduce the rate of slipping incidents (Bell et al., 2018; Verma et al., 2011) indicating that footwear is a promising type of personal protective equipment for falls.

One barrier that impedes the selection of appropriate slip-resistant footwear by employers and consumers is the expense and expertise that current shoe traction testing requires. Currently, experimental methods used to assess available coefficient of friction (ACOF) rely on expensive mechanical devices. This expense limits access to these methods. Given the compelling evidence that ACOF is affected by footwear tread design features, a valid assessment tool to predict ACOF values based on the outsole design features could be a useful alternate approach. This may provide safety practitioners with the opportunity to select higher performance slip-resistant shoes through these assessments and reduce worker's slip propensity. The development of observational tools has particular potential given the infrequent use of hardware-based methods. A recent survey revealed that only 14.8% of the safety practitioners utilized slipmeters to evaluate slip risk (Lowe et al., 2018). The study by Lowe et al. (2018) was a follow-up to the survey conducted by Dempsey et al. (2005), which indicated that 21.4% of practitioners used slipmeters. Use of slipmeters to *assess footwear* is probably even lower than the use of tribometers in general given that whole shoe tribometers are more expensive and less portable than floor tribometers (Chang et al., 2001b). An inexpensive observational assessment tool may increase the use of ergonomic tools by practitioners to address slip-related injuries.

One challenge in developing models that evaluate shoe traction is that different tribology mechanisms contribute to shoe-floor-contaminant friction, which makes the relationship between shoe outsole parameters and ACOF non-linear. For instance, an increase in contact area is generally associated with an increase in ACOF (Jones et al., 2018). However, a shoe outsole that achieves high contact area by eliminating all tread channel features is likely to operate in hydrodynamic lubrication (interacting surfaces are separated by a thin fluid film)

* Corresponding author.306 Schenley Place, 4420 Bayard Street, Pittsburgh, PA, 15213, United States.
E-mail addresses: ari16@pitt.edu (A. Iraqi), nvidic@pitt.edu (N.S. Vidic), mredfern@pitt.edu (M.S. Redfern), beschorn@pitt.edu (K.E. Beschorner).

https://doi.org/10.1016/j.apergo.2019.102963
Received 24 January 2019; Received in revised form 22 September 2019; Accepted 23 September 2019
Available online 1 November 2019

(Singh and Beschorner, 2014a). Hydrodynamic lubrication would reduce ACOF (Beschorner and Singh, 2012a; Hemler and Beschorner, 2017) despite a large contact area. Thus, the relationship between contact area and ACOF may not be monotonic when considering multiple lubrication regimes. This challenge can possibly be overcome by restricting the scope of assessment such that only a single tribology mechanism is present. In this study, we aim to focus only on hysteresis friction (friction caused by deformation of the elastomer) operating in boundary lubrication. ACOF values at boundary lubrication where hysteresis friction is presumably dominant may still pose a slip risk (Beschorner and Singh, 2012a; Jones et al., 2018). Moreover, shoes with a presence of tread drainage channels generally operate in boundary lubrication (Beschorner et al., 2014; Singh and Beschorner, 2014a). Hysteresis is the dominant mechanism in the presence of high viscosity fluids like glycerol and oils (Cowap et al., 2015; Jones et al., 2018; Strobel et al., 2012). Therefore, a wide range of conditions (shoes with drainage channels operating in the presence of high viscosity fluids) can be represented within this single tribology mechanism.

In the boundary lubrication regime, certain tread features have been shown to correlate with the ACOF. Previous research has indicated that shoe outsole features that influence contact pressures are correlated with hysteresis friction (Moghaddam et al., 2018). Specifically, lower contact pressures tend to increase hysteresis friction (Moghaddam et al., 2018). Tread surface area (i.e. the area of a treaded shoe in contact with the surface and previously referred to as "contact area" in Jones et al. (2018)) positively impacts ACOF (Jones et al., 2018; Moghaddam et al., 2018) since increased contact area leads to a reduction in contact pressures (Moghaddam et al., 2018). Also, increased material hardness negatively impacts ACOF (Cowap et al., 2015; Strobel et al., 2012) since softer material are subjected to higher deformations which increase contact area and reduce contact pressures (Moghaddam et al., 2018). Other outsole features that have been shown to affect hysteresis friction are heel shape (beveling or rounding in the sagittal plane) (Moghaddam and Beschorner, 2017) and heel width (in the frontal plane) (Jones et al., 2018). These may also be primarily explained by the changes in contact area (Moghaddam and Beschorner, 2017). Therefore, these outsole tread design features may form a basis for a tread assessment tool.

The objective of this study was to develop a statistical model to predict footwear traction based on observable outsole design features. The scope of the model is focused on shoe outsole tread that exhibit viscoelastic behavior and operate in boundary lubrication where hysteresis friction is dominant. The rationale for this study was that developing assessment tools based on cost-effective and easily evaluated measures of outsole tread will enable more occupational health and safety practitioners to assess footwear and improve workers' safety.

2. Materials and methods

This study consists of three main components: shoe outsole tread measurements, ACOF measurements, and statistical model building. Geometric and material measurements were made from the outsole tread of fifty-eight footwear designs. ACOF measurements were conducted using a robotic whole-shoe tester for these shoes against two types of flooring. A multiple linear regression model was developed using stepwise regression methods including k-fold cross-validation.

2.1. Materials

Sixty-three footwear that were marketed as slip-resistant from six brands (Shoes for Crews, Tredsafe, SR Max, SafeTstep, Dr. Scholl's, and Timberland PRO®) with low-collar height and laces were selected for this study (Table 1). No alternative footwear was included such as overshoes, slip-on, and clog shoe since wearing alternative footwear tends to lead to different slipping biomechanics (Chander et al., 2016) and may be inappropriate for the specified ACOF test methods. Slip-resistant footwear included casual, work, athletic and dress style

Table 1
List of slip-resistant shoes included in the study from different brands (Rows that are bold represent modified shoes).

Shoe Code	Brand	Model	Style/item #	Style	Gender
A1	Shoes for Crews	Cambridge	6006	Dress	M
A2		Condor	24734	Athletic	M
A3		Delray - Canvas	38852	Casual	M
A4		Creed	21771	Athletic	M
A5		Senator	1201	Dress	M
A6		Avery	34545	Athletic	F
A7		Old School Low-Rider IV - Leather	39362	Casual	F
A8		Heather	9048	Athletic	F
A2HS		**Condor**	**24734**	**Athletic**	**M**
A1HW		**Cambridge**	**6006**	**Dress**	**M**
A1CA		**Cambridge**	**6006**	**Dress**	**M**
A1SF		**Cambridge**	**6006**	**Dress**	**M**
B1	Tredsafe	Axel	555307251	Athletic	M
B2		Executive II	553701356	Work	M
B3		Mario	553996011	Athletic	M
B4		Engage	565589700	Casual	U
B5		Kitch Canvas	553926483	Work	U
B6		Rig	553802532	Casual	U
B7		Nitro	556595638	Athletic	M
B8		Bailey	553987412	Athletic	W
B1HS		**Axel**	**555307251**	**Athletic**	**M**
B1HW		**Axel**	**555307251**	**Athletic**	**M**
B1CA		**Axel**	**555307251**	**Athletic**	**M**
B1SF		**Axel**	**555307251**	**Athletic**	**M**
C1	SR Max	Arlington	SRM350	Dress Oxford	F
C2		Tampa	SRM125	Athletic Oxford	F
C3		Abilene	SRM400	Casual Oxford	F
C4		Portland	SRM621	Skate	F
C5		Maxton	SRM620	Athletic	F
C6		Fairfax	SRM1580	Low Athletic	M
C7		Rialto	SRM6000	Athletic Sneaker	M
C8		Atlanta	SRM3700	Oxford	M
C2HS		**Tampa**	**SRM125**	**Athletic Oxford**	**F**
C1HW		**Arlington**	**SRM350**	**Dress Oxford**	**F**
C1CA		**Arlington**	**SRM350**	**Dress Oxford**	**F**
C1SF		**Arlington**	**SRM350**	**Dress Oxford**	**F**
D1	safeTstep	Deidre	162446	Oxfords	F
D2		Camina	159959	Runner	F
D3		Andre	173851	Court	F
D4		Kandice	163896	Canvas Oxfords	F
D5		Blast	159961	Runner	F
D6		Zeus	174484	Athletic	M
D7		Monroe	160023	Oxfords	M
D8		Halfpipe	166413	Canvas Oxfords	M
D1HS		**Deidre**	**162446**	**Oxford**	**F**
D1HW		**Deidre**	**162446**	**Oxford**	**F**
D1CA		**Deidre**	**162446**	**Oxford**	**F**
D1SF		**Deidre**	**162446**	**Oxford**	**F**
E1	Dr. Scholl's	Proudest	88626	Oxford	M
E2		Intrepid	88622	Sneaker	M
E3		Aiden	25311	Work Sneaker	M
E4		Roberts	14064	Oxford	M
E5		Hiro	25318	Oxford	M
E6		Kimberly II	88755	Sneaker	F

(continued on next page)

Table 1 (*continued*)

Shoe Code	Brand	Model	Style/item #	Style	Gender
E7		Brave	88751	Sneaker	F
E8		Inhale	22876	Sneaker	F
E2HS		**Intrepid**	**88622**	**Sneaker**	**M**
E1HW		**Proudest**	**88626**	**Oxford**	**M**
E1CA		**Proudest**	**88626**	**Oxford**	**M**
E1SF		**Proudest**	**88626**	**Oxford**	**M**
F1	Timberland PRO	PRO-232	$54.2 \pm 2.3^{\Psi}$	Work	M
F2		PRO-232	$60.4 \pm 1.5^{\Psi}$	Work	M
F3		PRO-232	$63.2 \pm 2.4^{\Psi}$	Work	M

Ψ shore A hardness.
HS modified to control heel shape.
HW modified to control heel width.
CA modified to control tread surface area.
SF modified to control shape factor.

that were marketed as men's, women's, and unisex shoes. Shoe selection was aimed to achieve variation in outsole geometry and material hardness between and within shoe brands. Twenty of the selected footwear (four per each brand, except Timberland PRO®) were modified to systematically control outsole geometry. Three pairs of shoes were custom made to have identical outsole tread geometry but with different levels of material hardness (F1, F2, F3). All sixty-three footwear were US size 9 men's shoe or the equivalent size for women's shoes.

Footwear outsole features such as material hardness (Jones et al., 2018; Tsai and Powers, 2008), tread surface area (Jones et al., 2018; Moghaddam et al., 2018), heel width (Jones et al., 2018) and heel shape (Moghaddam and Beschorner, 2017) were selected for measurements based on their association with hysteresis friction from previous research. Additionally, shoe outsole metrics were selected to be low-cost in order to make the assessment accessible to practitioners (Table 2). For instance, a dynamic mechanical analyzer provides viscoelastic properties of elastomers (Wang et al., 2011), which may be linked to hysteresis friction (Lindner et al., 2004; Wang et al., 2011). However, this device can cost over $10,000 whereas a Shore A durometer costs about $30 (Table 2). Additionally, shape factor (i.e., the loaded area of a rubber block divided by its area of lateral surface free to bulge) was considered since shape factor has been found to affect the deformability of the rubber block in other tribology applications (elastomeric bearings and tire tread) (Imbimbo and De Luca, 1998; Sridharan and Sivaramakrishnan, 2012). We hypothesized that the shape factor of the individual tread will affect the ACOF since it influences the deformability of the tread.

Table 2
Shoe outsole, floor surface and lubricant properties that may contribut to friction. The parameters included in this study are italicized (Tread depth was incorporated in the calculation of shape factor).

Parameters	Apparatus	Cost (U.S. dollars)[a]
Shoe outsole		
Heel shape (sagittal plane)	Visual observation	NA
Heel width (frontal plane)	Ruler[c]	5
Material hardness	Shore A durometer[d]	30
Mechanical properties	Dynamic Mechanical Analyzer[e, b]	10000
Surface roughness	Stylus profilometer[f]	1500
Tread depth	Digital caliper[g]	10
Tread surface area (top)	Shoe imprint using ink pad[h]	10
Lubricant		
Viscosity	Rotary Viscometer[i]	500
Floor		
Surface roughness	Stylus profilometer[f]	1500
Shoe-floor-lubricant		
Contact area/pressure	Pre-scale pressure sensitive film[j]	500
Surface free energy	Contact angle meter[k]	1000

[a] Actual costs vary according to brand, vendor, and exact device that is purchased.
[b] Price based on used equipment.
[c] (Amazon, 2019e).
[d] (Amazon, 2019b).
[e] (eBay, 2019)
[f] (Google, 2019b).
[g] (Amazon, 2019a).
[h] (Amazon, 2019c).
[i] (Amazon, 2019d).
[j] (Google, 2019a).
[k] (Neobits, 2019).

The Shore A material hardness of five different treads per shoe was measured using a durometer (ASTM D2240-15, 2015). A mass of 1 kg was affixed and centered on the axis of the indentor as recommended by the ASTM D2240-15 (2015) to improve repeatability of handheld measurements and additionally shoes were secured using a bench vise during measurements. The tread surface area of the heel was measured using an ink pad, a white blank sheet of paper and a scanner (Jones et al., 2018; Tencer et al., 2004). Ink was applied to the outsole and the outsole was firmly pressed over a white blank sheet of paper. At least three imprints per shoe were created to ensure that pressure was applied across the entire heel section of the outsole and the heel imprint that had the maximum inked area was selected. The heel imprint was scanned and a MATLAB script (MATLAB, MathWorks®, Natick, MA) was developed to calculate the tread surface area (black region, Fig. 1). The posterior-most point of the tread to 5 cm anterior of that point was used for calculation of the tread surface area (Fig. 1) (Jones et al., 2018). The heel width and dimensions of the tread blocks were measured using a ruler and digital caliper, respectively. The heel width was measured 1.5 cm anterior of the posterior-most point of the tread (Fig. 1) (Jones et al., 2018). Shoe beveling features were observed by placing the shoe on a level surface. The heel of the outsole was categorized as flat-edge or beveled edge if the heel was parallel to the level surface or formed a convex shape with respect to the leveled surface, respectively. The shape factor (S) was calculated based on the tread geometry at five different locations (Eq. (1)) (Imbimbo and De Luca, 1998). If the shape of the tread geometry varied across the heel, only the shape of the tread geometry that was dominant in the 1.5 cm most posterior section of the tread was considered for shape factor calculation. The loaded area was defined as the top surface area of a tread that was subjected to the normal load and the surface area free to bulge was considered as the lateral surface area of a tread (Fig. 2). Sipes, which are cuts and groves on the tread surface, were neglected during this calculation (Fig. 2).

$$S = \frac{Loaded\ area}{Surface\ area\ free\ to\ bulge} \quad \text{(Eq. 1)}$$

Four footwear from each brand (except Timberland PRO®) were altered to systematically vary tread surface area (A1CA-E1CA), heel width (A1HW-E1HW), shape factor (A1SF-E1SF) and heel shape (A2HS, B1HS, C2HS, D1HS, E2HS) within brands (Fig. 3). (1) One flat-edge footwear per brand had tread removed at the midline (A1CA-E1CA). (2) One flat-edge footwear per brand had individual tread removed at the outer edge (A1HW-E1HW). (3) One beveled edge footwear had individual tread removed (A2HS, C2HS, E2HS) to approximate the heel width and tread surface area of the corresponding flat-edge footwear (A1, C1, E1) if the beveled edge had higher tread surface area than the flat-edge shoe. Otherwise the flat-edge shoe had tread removed (B1HS, D1HS) to closely match the heel width and tread surface area of the corresponding beveled edge footwear (B2, D2). (4) One flat-edge footwear per brand had tread depth shortened (about 1 mm) by abrasion on a belt sander with 36 grit belt (A1SF-E1SF). Modification 1 and 2 allowed for tread surface area and heel width to be systematically modified while keeping the heel shape, shape factor and material hardness consistent across shoes. Modification 3 allowed to discern the effect of heel shape while keeping the shape factor, material hardness, tread surface area and heel width consistent across shoes. Modification 4

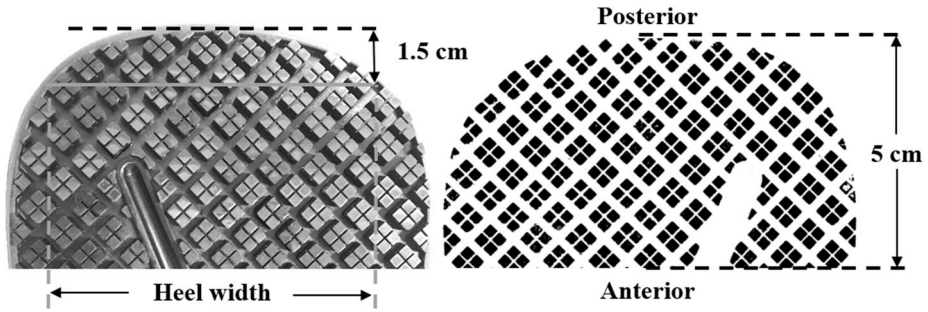

Fig. 1. Heel width (left) was measured across the shoe heel with a ruler. The tread surface area (right) was measuremed using an ink impring of the posterior 5 cm of the shoe tread.

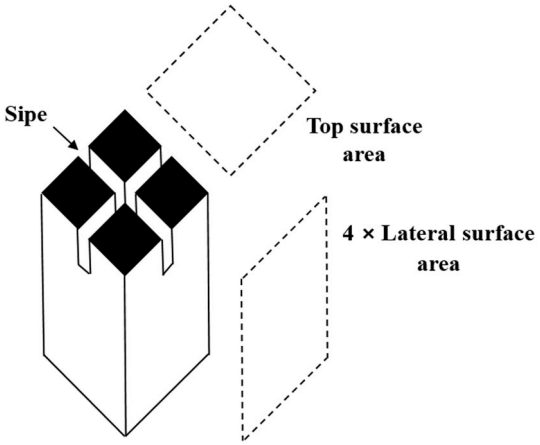

Fig. 2. Shape factor measurement of a tread (black region represents tread surface area).

modified the shape factor by decreasing the tread depth. Roughness measurements were taken after abrasion to monitor the surface roughness of the abraded shoes with respect to the new shoes. Five roughness measurements on five different treads were recorded for each shoe in the direction of the shoe motion using a stylus profilometer (Surtronic S128, Taylor-Hobson®, AMETEK®, Leicester, United Kingdom). The scan length and cutoff frequency during roughness measurements of the tread surface were 1.6 mm and 0.8 mm, respectively. The abrasion caused significant changes to the shoe tread surfaces (A1SF-E1SF). The average peak to valley height (R_z) for new shoes and abraded shoes (A1SF-E1SF) were 13.2 ± 5.7 μm and 47.1 ± 14.5 μm, respectively. The abraded shoes (A1SF-E1SF) were excluded *a priori* to the statistical analysis since surface roughness was a confounding factor with shape factor.

The materials used for ACOF testing were canola oil and two floor designs. Canola oil was used as the liquid contaminant to simulate a common workplace contaminant in the service industry. A high and low traction tile were used for flooring condition: (1) ceramic tile (model: ADJF250802, make: ASTM), and (2) high pressure laminate tile (model: 00503 Stone Grafix, make: Formica®), respectively. Five roughness measurements were recorded for each tile in the direction of the shoe motion using the stylus profilometer. The scan length and cutoff frequency during roughness measurements were 8 mm and 0.8 mm, respectively. The average ± standard deviation of the peak to valley height (R_z), arithmetic average (R_a), root mean square (R_q), and root mean square of surface slope (R_{dq}) for the ceramic/laminate tile were $22.2 \pm 1.4/17.0 \pm 0.9$ μm, $3.9 \pm 0.3/3.1 \pm 0.3$ μm, $5.1 \pm 0.3/3.9 \pm 0.3$ μm, and $29.9 \pm 0.3/28.8 \pm 0.1°$, respectively. A total of 116 footwear-floor-contaminant combinations (58 footwear * 1 liquid contaminant * 2 floor surfaces) were tested.

2.2. ACOF measurements

A robotic friction measurement device, i.e., Portable Slip Simulator (Aschan et al., 2005; Iraqi et al., 2018), was used to measure the ACOF between the footwear outsole and floor surface in the presence of the contaminant. A 6 degree-of-freedom force plate (BERTEC Corporation, Columbus, OH, USA) with the floor tile mounted on top was used to record ground reaction forces with a sampling frequency of 500 Hz.

The ACOF testing parameters were an average normal force of 250 ± 10 N, shoe-floor angle of $17 \pm 1°$ and sliding speed of 0.5 m/s. The 250 N, 17°, 0.5 m/s was selected based on the set of testing parameters that best predicted slip outcomes in a previous study (Iraqi et al., 2018). The shoe-floor angle was measured when the shoe was fully loaded and forefoot was rotated to 17°. The shoe angle was with respect to the shoe's orientation when the shoe was unloaded and placed on the floor (Jones et al., 2018). Five repeated trials were carried out for each shoe-floor combination.

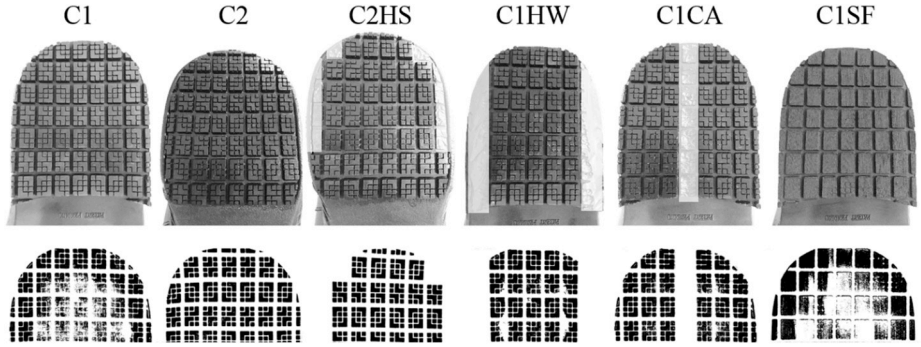

Fig. 3. A representative set of shoe samples being modified and their corresponding tread surface area. Grey area on the shoe outsole (top) represents regions where individual treads were removed.

2.3. Data and statistical analysis

The ACOF was quantified as the ratio of resultant shear force to normal force (Eq. (2)) (Iraqi et al., 2018; Siegmund et al., 2006). The ACOF was averaged over the first 200 ms after 250 N was reached. The average normal force was within ±10 N of 250 N and the range of normal force was within 10% (25 N) of 250 N during this 200 ms interval (Iraqi et al., 2018).

$$ACOF = \frac{\sqrt{F^2_{Longitudinal\ Shear} + F^2_{Transverse\ Shear}}}{F_{Normal}} \quad \text{(Eq. 2)}$$

A multiple linear regression model was developed to predict ACOF in the presence of canola oil based on the tread features while controlling for the floor type. The independent variables were as follows: material hardness, tread surface area, heel width, shape factor, heel shape, floor type, and all first-order interactions. The heel shape and floor type were modeled as categorical variables.

The model's overall significance was tested using the ANOVA method for multiple linear regression. Tests on individual regression coefficients (relative to zero) were performed using t-tests. A backward elimination method was used to screen the candidate regressors (predictors) and eliminate regressors (predictors) that have negligible effects. Additionally, forward selection and hybrid method were performed to determine if the model building approach influenced the parameters resulting in the model. A k-fold cross-validation method (k = 5) was used to select the optimal model (i.e., to only select the predictors in the model that minimize the cross-validation error). The 5-fold cross-validation method was repeated five times for each model size since cross-validation error changes due to different split of data in the cross-validation folds. The model was selected based on the one-standard-error-rule (i.e., cross-validation error is within one standard error of the lowest point on the curve) (James et al., 2013). The cross-validation method assessed how well the trained models predicted an independent data set. The advantage of the k-fold cross-validation is that each subset of data is used for both training (i.e., estimation) and testing (i.e., validation) (James et al., 2013). Residual analysis was performed to ensure that the normality and homoscedasticity assumptions of the regression model were met. A Shapiro-Wilk test was used to test if the ACOF residuals from the model followed were following a normal distribution. The statistical analyses were performed using commercial software (JMP® Pro 14.0.0, SAS Institute Inc., Cary, NC, USA) with a significance level of 5%.

3. Results

The shoes were evenly distributed between beveled edge (50%, 29 shoes) and flat-edge (50%, 29 shoes) heel shapes. The shore A hardness and shape factor values ranged from 44.2 to 65.6 and from 0.19 to 0.91, respectively. The tread surface area ranged from 6.36 to 16.08 cm^2 (same range without modified shoes). The heel width was between 3.8 cm and 7.4 cm (5.0–7.4 cm without the modified shoes). The ACOF values for the 43 shoes (excluding the modified shoe outsoles) with

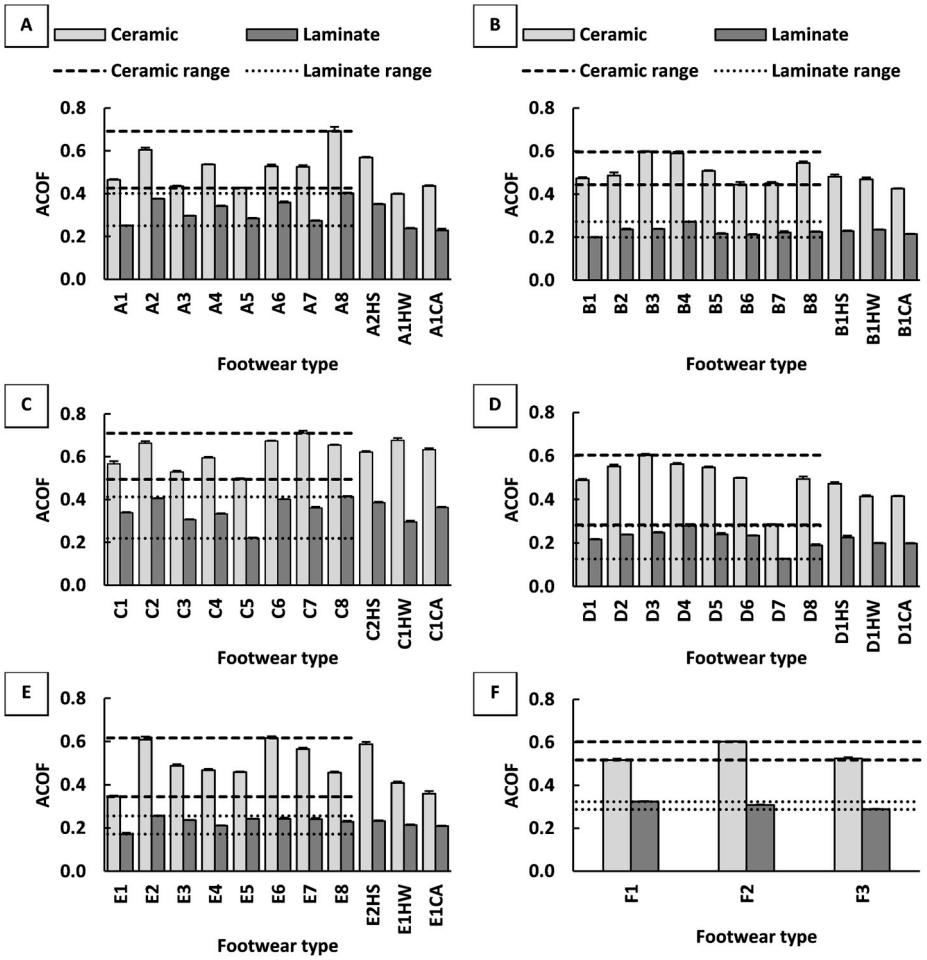

Fig. 4. ACOF for ceramic (light grey) and laminate (dark grey) tile with canola oil for the shoe brands: (A) Shoes for Crews, (B) Tredsafe, (C) SR Max, (D) safeTstep, (e) Dr. Scholl's, and (F) Timberland PRO. The dashed lines and dotted lines on each plot show the range of ACOF within brands (for unmodified shoes) on both ceramic and laminate tile, respectively.

ceramic and laminate tile ranged from 0.283 (D7) to 0.710 (C7) and 0.127 (D7) to 0.413 (C8), respectively (Fig. 4A–F). The ACOF for the 15 modified shoes ranged from 0.358 (E1CA) to 0.677 (C1HW) for ceramic tile and 0.197 (D1CA) to 0.385 (C2HS) for laminate tile, which were within the ACOF range of unmodified shoes on the corresponding floorings. All shoes had higher ACOF on ceramic tile compared to laminate tile (Fig. 4).

The ACOF was significantly predicted by the full model that included all predictors (material hardness, tread surface area, heel width, shape factor, heel shape, floor type, and all first-order interactions, $F_{21,94} = 37.2$, $p < 0.001$). The *t*-test performed on the individual regression coefficients indicated that the heel shape (beveled: $t_{95} = 3.44$, $p = 0.001$), tread surface area ($t_{95} = 3.81$, $p < 0.001$), hardness ($t_{95} = -2.31$, $p = 0.023$), floor type (ceramic: $t_{95} = 25.08$, $p < 0.001$), and the interaction between the heel shape and shape factor ($t_{95} = -2.26$, $p = 0.023$) were statistically significant. The heel width ($t_{95} = -0.64$, $p = 0.524$) and shape factor ($t_{95} = 1.36$, $p = 0.176$) were insignificant in the full model. This model explained 89% ($R^2 = 0.893$, $R^2_{adj} = 0.869$, RMSE = 0.054) of the variation in ACOF based on the full set of predictor variables.

The backward elimination method resulted in a reduced model ($F_{6,109} = 135.3$, $p < 0.001$, Eq. (3)) and included the heel shape ($t_{110} = 3.37$, $p = 0.001$), tread surface area ($t_{110} = 4.92$, $p < 0.001$), hardness ($t_{110} = -2.93$, $p = 0.004$), shape factor ($t_{110} = 3.15$, $p = 0.002$), floor type ($t_{110} = 25.73$, $p < 0.001$), and the interaction between the heel shape and shape factor ($t_{110} = -2.42$, $p = 0.017$) (Table 3). The heel width and other first-order interactions were removed in the reduced model by the backward elimination method. The forward selection method resulted in a reduced model ($F_{4,111} = 187.1$, $p < 0.001$, Eq. (4)) that included four of the six factors that were part of the model identified through the backward elimination method. The model resulting from the forward selection method included the heel shape ($t_{112} = 3.48$, $p = 0.001$), tread surface area ($t_{112} = 5.26$, $p < 0.001$), hardness ($t_{112} = -2.64$, $p = 0.009$), and floor type ($t_{112} = 24.86$, $p < 0.001$) (Table 3). The heel width, shape factor and all first-order interactions were not added to the model via the forward selection method. The hybrid method resulted in the same model as the backward elimination method. A slightly lower standard error was achieved with 6 predictors (i.e. backward elimination model) than what was achieved with 4 predictors (i.e., forward selection model) (Fig. 5). While the model with 6 predictors (Eq. (3)) was considered the optimal model based on this criterion, the model with 4 predictors (Eq. (4)) was nearly as strong, did not include any interaction effects, and required one fewer measurement. In Eq. (3), the units are represented in brackets for continuous variables. Nominal dummy variables are set to a value of 1 when the condition within the brackets is present and 0 when the condition within the brackets is not present. The predictor variables in the optimal/backward elimination model explained 88.2% ($R^2 = 0.882$, $R^2_{adj} = 0.875$, RMSE = 0.053) of the variation in ACOF (Supplemental Fig. 1). The forward selection model explained 87.1%

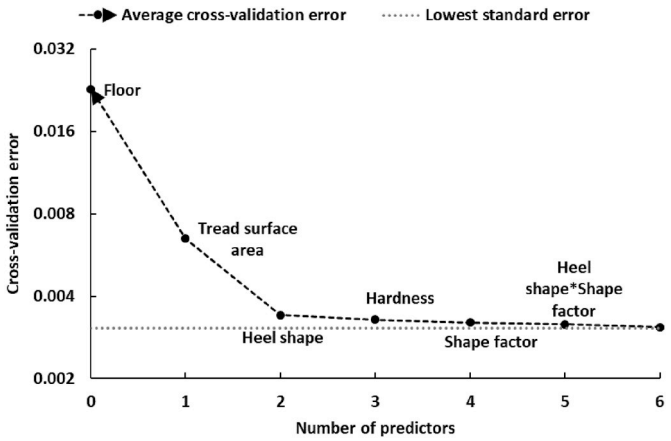

Fig. 5. Cross-validation error for different number of significant predictors in the reduced models The data label above/below each data point indicates which parameter was removed during backward elimination. Standard error for each data point is small, which is not visible on the plot.

($R^2 = 0.871$, $R^2_{adj} = 0.866$, RMSE = 0.055) of the variation in ACOF (Fig. 6). The normal quantile plot for the backward (Supplemental Fig. 2A) and forward model indicated no extreme violations of the normality assumption (Fig. 7A). Additionally, the Shapiro-Wilk test indicated that the ACOF residuals follow a normal distribution ($W = 0.985$, $p = 0.224$). The plot of the residual vs. predicted ACOF did not exhibit any extreme unusual patterns that suggest violations of

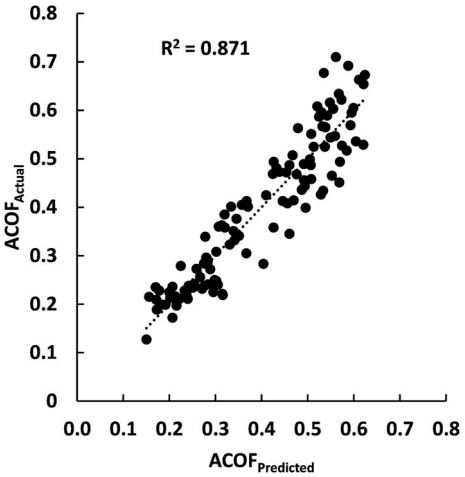

Fig. 6. Actual vs. predicted ACOF (response variable) from the forward model (Eq. (4)).

Table 3
Summary of parameter estimates (95% confidence interval: CI and standard error: Std error) for the backward elimination (column 2–4) and forward selection (column 5–7) model. NA represents variables that were not part of the model.

	Backward elimination			Forward selection		
Terms	β (CI)	Std error	*t*-test (p-value)	β (CI)	Std error	*t*-test (p-value)
Intercept	0.158 (−0.003 to 0.320)	0.082	1.94 (0.055)	0.223 (0.064–0.383)	0.081	2.77 (0.007)
Heel shape[beveled]	0.130 (0.054–0.207)	0.039	3.37 (0.001)	0.041 (0.018–0.064)	0.012	3.48 (0.001)
Floor[ceramic]	0.254 (0.234–0.273)	0.010	25.73 (<.001)	0.254 (0.234–0.274)	0.010	24.86 (<.001)
Tread surface area (cm^2)	0.014 (0.008–0.020)	0.003	4.92 (<.001)	0.015 (0.009–0.021)	0.003	5.26 (<.001)
Heel width (cm)	NA	NA	NA	NA	NA	NA
Shape factor	0.160 (0.059–0.261)	0.051	3.15 (0.002)	NA	NA	NA
Hardness	−0.003 (−0.005 to −0.001)	0.001	−2.93 (0.004)	−0.003 (−0.005 to −0.001)	0.001	−2.64 (0.009)
Heel shape[beveled] *Shape factor	−0.154 (−0.280 to −0.028)	0.064	−2.42 (0.017)	NA	NA	NA
Other first order interactions	NA	NA	NA	NA	NA	NA

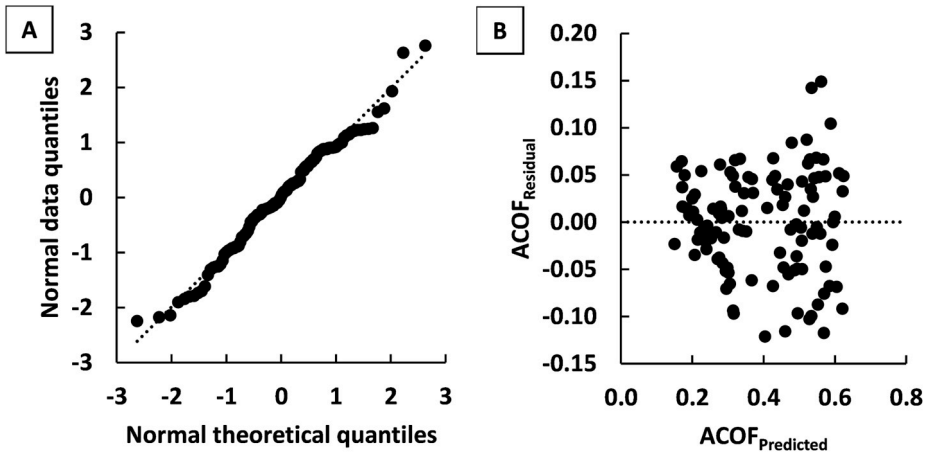

Fig. 7. Residual analysis performed on the forward model: (A) normal quantile plot to assess the assumption of normality; and (B) plot of residual vs. predicted ACOF to assess assumption of homoscedasticity.

homoscedasticity assumption for either model (Fig. 7B and Supplemental Fig. 2B).

$$\begin{aligned} \textit{Backward elimination}: \ ACOF &= 0.158 + 0.014 * \textit{tread surface area}\left[cm^2\right] + 0.130 * \textit{heel shape} - 0.003 * \textit{hardness}\left[\textit{Shore A}\right] \\ &+ 0.160 * \textit{shape factor} + 0.254 * \textit{floor} - 0.154 * \textit{heel shape} * \textit{shape factor} \end{aligned} \quad \text{(Eq. 3)}$$

$$\begin{aligned} \textit{Forward selection}: \ ACOF &= 0.223 + 0.015 * \textit{tread surface area}\left[cm^2\right] \\ &+ 0.041 * \textit{heel shape} - 0.003 * \textit{hardness}\left[\textit{Shore A}\right] \\ &+ 0.254 * \textit{floor} \end{aligned} \quad (4)$$

According to the regression coefficients from the forward model (Table 3), a unit increase in the tread surface area (cm^2) increased the ACOF by 0.015 ($\beta_{\text{Tread surface area}}$). An increase in the tread surface area from the first quartile (9.6) to the third quartile (13.4) increased ACOF by 0.057 (interquartile range * $\beta_{\text{Tread surface area}} = 3.8 * 0.015$). A unit increase in the Shore A hardness decreased the ACOF by 0.003 (β_{Hardness}). An increase in the Shore A hardness from the first quartile (49.8) to the third quartile (60.8) reduced ACOF by 0.033 (interquartile range * $\beta_{\text{Hardness}} = 11.0 * -0.003$). The change from flat-edge to beveled edge heel shape increased ACOF by 0.041 ($\beta_{\text{Heel shape[beveled]}}$). The change of floor type from laminate to ceramic tile added 0.254 ($\beta_{\text{Floor [ceramic]}}$) to the ACOF.

4. Discussion

The main finding of this study was that simple and relatively inexpensive measurements of footwear outsole tread could predict the variation in oily traction performance across shoes labeled as slip-resistant. This finding indicated that tread geometry (heel shape and tread surface area) and material hardness, while controlling for floor type, explained 87% of the variation in oily ACOF. Change in heel shape from flat to beveled edge and increase in tread surface area were favorable in the traction performance within each brand. Moreover, the prediction of ACOF was based on mostly main effects. Only a single interaction term (heel shape*shape factor, p-value = 0.017) was observed and this interaction effect was only observed in two of the three stepwise regression models. These findings have two-fold benefits. First, assessment of slip-resistant shoes based on regression model predictions will be possible for safety practitioners without actually performing experimental shoe traction testing. Second, footwear manufacturers can improve shoe traction by prioritizing heel shape (flat to beveled edge) and tread surface area.

The relationship between shoe outsole tread, floor type, and ACOF in the current study are generally in agreement with previous research. The tread surface area was positively associated with ACOF, consistent with previous findings (Jones et al., 2018; Moghaddam et al., 2018). As the tread surface area increases, contact pressures reduce and consequently cause an increase in hysteresis friction (Moghaddam et al., 2018). The higher ACOF values associated with beveled edge heel shape compared to flat edge were also consistent with findings of Moghaddam and Beschorner (2017). A beveled edge increases the area of contact by conforming the tread to the floor when the shoe is at an angle during the early stages of stance. This has a positive impact on ACOF. The effect of material hardness on ACOF has been also supported by previous research (Cowap et al., 2015; Jones et al., 2018; Strobel et al., 2012; Tsai and Powers, 2008) since hardness contributes to hysteresis friction in the presence of high viscous lubricants (Cowap et al., 2015; Strobel et al., 2012). The softer elastomer (low hardness level) will be subjected to higher deformation compared to the harder material, which increases ACOF (Strobel et al., 2012). Furthermore, the floor surface with a higher roughness was associated with a higher ACOF, which has been demonstrated in previous research (Chang et al., 2001a; Cowap et al., 2015; Moghaddam et al., 2015).

The statistical model predicting footwear traction based on simple and inexpensive measurements of outsole tread may be a useful assessment tool. Tread surface area was measured with an ink pad, paper and scanner. Heel shape was visually observed without the use of any equipment. Hardness was measured using a durometer that costs approximately US $30 (Table 1). A safety manager could measure these parameters and use the developed model to screen out slip-resistant shoes that pose a high or moderate slip risk. For instance, the model differentiated between shoes with high and low ACOF across brands similar to the ACOF yielded through experiments (Fig. 8). The study revealed that certain shoes with low ACOF show evidence of poor outsole backing design that result in gaps in tread surface area compared with other designs within the same brand (Fig. 8, left). Thus, the

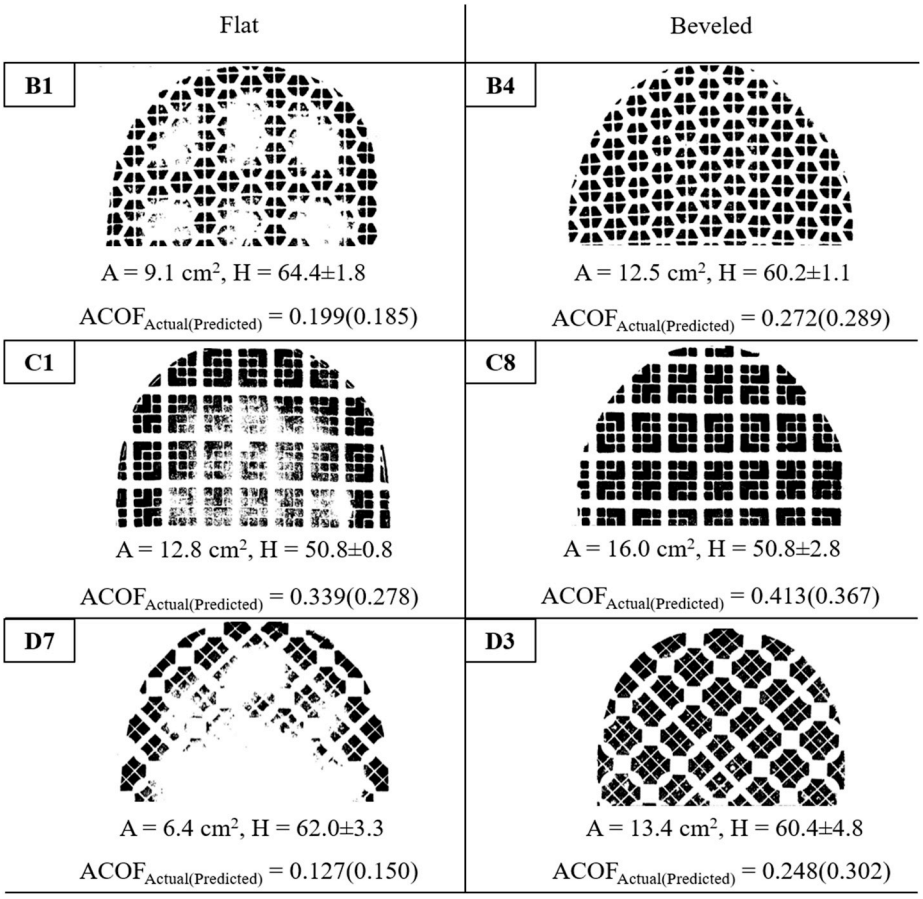

Fig. 8. A comparison of ACOF across heel designs within brands (B, C, D) on laminate tile. ACOF is labeled for the measured value (Actual) as well as the model-predicted value (Predicted) based on Eq. (4) (forward model). The ACOF is relatively higher for the designs in column one (B4, C8, D3) compared to their corresponding shoe brand (B1, C1, D7) in column two primarily due to higher tread surface area and beveled edge heel shape. (A and H represent tread surface area and Shore A hardness, respectively.)

observational methods described in this study may help to differentiate across shoes with higher and lower slip-resistant properties. About 70% of unmodified shoes tested on laminate tile had ACOF below 0.30. An ACOF level above 0.30 (Grönqvist et al., 1989) or 0.29 (ANSI/NFSI B101.7, 2018) has been suggested for safe level walking. Also, the range of ACOF values (0.127–0.413) for laminate tile had overlap with RCOF range (0.155–0.272) for level walking (Beschorner et al., 2016; Perkins and Wilson, 1983; Redfern and DiPasquale, 1997). Furthermore, recent research has demonstrated that interventions that only permit high performance slip-resistant shoes can dramatically reduce the odds of slipping compared with interventions where employees can select any slip-resistant footwear (Bell et al., 2018). Thus, this study operated in conditions where the differences in shoe performance are relevant and where identifying high performance slip-resistant shoes could reduce fall injuries.

Certain limitations of the current study should be acknowledged. Only two different floorings were utilized and flooring was treated as a categorical variable in the regression analysis instead of by its physical characteristics. Future research that incorporates physical characteristics of flooring such as multiscale surface roughness (Moghaddam et al., 2018) and spreading coefficient (Nishi et al., 2016; Shibata et al., 2019) into the statistical model to predict traction would be beneficial. It is worth noting that interaction effects including flooring were small and insignificant. Furthermore, other research has suggested that shoe traction performance across vinyl composite, quarry and ceramic floor surfaces are generalizable in the presence of canola oil (Chanda et al., 2018). Thus, these results are expected to be consistent when applied to other floorings. Moreover, the liquid contaminant used was canola oil which allowed this study to focus primarily on hysteresis friction mechanisms within boundary lubrication. Further investigations are required to understand the generalizability to other liquid contaminants such as water and detergent aqueous solution. Another limitation is that this model should not be used to predict ACOF beyond the range of predictors that were used to develop the model (Shore A hardness: 44.2–65.6; shape factor: 0.19–0.91, heel shape: flat or beveled edge, tread surface area: 6.36–16.08 cm^2). This study only included shoes with tread that were presumed to operate in boundary conditions and may not be applicable to non-slip resistant or worn shoes that may operate in other lubrications regimes like hydrodynamic lubrication (Beschorner et al., 2014; Singh and Beschorner, 2014a). Lastly, the model may not be applicable to foot slips on ladder rung, stair walking, or running conditions.

5. Conclusion

In summary, the current study suggests that slip-resistant shoes with a beveled heel shape, higher tread surface area, and lower material hardness generate higher traction in the presence of canola oil. Furthermore, a multiple regression model was generated that predicted ACOF based on these parameters. This type of predictive model may be useful to safety practitioners to select higher traction performance shoes.

Acknowledgements

Funding for this study was provided by the National Institute for Occupational Safety and Health (NIOSH R03OH011069 and R01OH010940), Custom footwear provided by VF Corporation®.

Appendix A. Supplementary data

Supplementary data to this article can be found online at https://doi.org/10.1016/j.apergo.2019.102963.

References

Amazon, 2019. Digital Caliper. Retrieved from. https://www.amazon.com/s?k=digital+caliper&i=industrial&ref=nb_sb_noss.

Amazon, 2019. Handheld Shore A Durometer. Retrieved from https://www.amazon.com/s?k=handheld+shore+A+durometer&i=industrial&ref=nb_sb_noss.

Amazon, 2019. Inkpad. Retrieved from. https://www.amazon.com/s?k=inkpad&ref=nb_sb_noss.

Amazon, 2019. Rotary Viscometer. Retrieved from. https://www.amazon.com/s?k=Rotary+Viscometer&i=industrial&s=relevancerank&qid=1561056995&ref=sr_st_relevancerank.

Amazon, 2019. Ruler. Retrieved from. https://www.amazon.com/s?k=ruler&ref=nb_sb_noss_1.

ANSI/NFSI draft B101.7, 2018. Standard test method for lab measurement of footwear heel outsole material coefficient of friction on liquid-contaminated floor surfaces. In: NFSI Standards Committee B101 Safety Requirements for Slip, Trip and Fall Prevention.

Aschan, C., Hirvonen, M., Mannelin, T., Rajamäki, E., 2005. Development and validation of a novel portable slip simulator. Appl. Ergon. 36 (5), 585–593.

ASTM D2240-15, 2015. Standard test method for rubber property - durometer hardness. ASTM International, West Conshohocken, PA.

Bell, J.L., Collins, J.W., Chiou, S., 2018. Effectiveness of a No-Cost-To-Workers, Slip-Resistant Footwear Program for Reducing Slipping-Related Injuries in Food Service Workers: a Cluster Randomized Trial. Scand. J. Work Environ. Health.

Bell, J.L., Collins, J.W., Wolf, L., Grönqvist, R., Chiou, S., Chang, W.-R., et al., 2008. Evaluation of a comprehensive slip, trip and fall prevention programme for hospital employees. Ergonomics 51 (12), 1906–1925.

Beschorner, K.E., Albert, D.L., Chambers, A.J., Redfern, M.S., 2014. Fluid pressures at the shoe–floor–contaminant interface during slips: effects of tread & implications on slip severity. J. Biomech. 47 (2), 458–463.

Beschorner, K.E., Albert, D.L., Redfern, M.S., 2016. Required coefficient of friction during level walking is predictive of slipping. Gait Posture 48, 256–260.

Beschorner, K.E., Singh, G., 2012. A novel method for evaluating the effectiveness of shoe-tread designs relevant to slip and fall accidents. In: Paper Presented at the Human Factors and Ergonomics Society. Boston, MA.

Chanda, A., Jones, T.G., Beschorner, K.E., 2018. Generalizability of footwear traction performance across flooring and contaminant conditions. IISE Trans. Occup. Ergon. Human Factors 6 (2), 98–108.

Chander, H., Wade, C., Garner, J.C., Knight, A.C., 2017. Slip initiation in alternative and slip-resistant footwear. Int. J. Occup. Saf. Ergon. 1–12. https://www.tandfonline.com/doi/abs/10.1080/10803548.2016.1262498.

Chang, W.-R., Kim, I.-J., Manning, D.P., Bunterngchit, Y., 2001. The role of surface roughness in the measurement of slipperiness. Ergonomics 44 (13), 1200–1216. https://doi.org/10.1080/00140130110085565.

Chang, W.R., Gronqvist, R., Leclercq, S., Brungraber, R.J., Mattke, U., Strandberg, L., et al., 2001. The role of friction in the measurement of slipperiness, Part 2: survey of friction measurement devices. Ergonomics 44 (13), 1233–1261. Retrieved from 11794766.

Courtney, T.K., Sorock, G.S., Manning, D.P., Collins, J.W., Holbein-Jenny, M.A., 2001. Occupational slip, trip, and fall-related injuries-can the contribution of slipperiness be isolated? Ergonomics 44 (13), 1118–1137. https://doi.org/10.1080/00140130110085538.

Cowap, M.J.H., Moghaddam, S.R.M., Menezes, P.L., Beschorner, K.E., 2015. Contributions of adhesion and hysteresis to coefficient of friction between shoe and floor surfaces: effects of floor roughness and sliding speed. Tribol. Mater. Surf. Interfaces 9 (2), 77–84. https://doi.org/10.1179/1751584X15Y.0000000005.

Dempsey, P.G., McGorry, R.W., Maynard, W.S., 2005. A survey of tools and methods used by certified professional ergonomists. Appl. Ergon. 36 (4), 489–503.

eBay, 2019. Perkin Elmer Dynamic Mechanical Analyzer Dma 7 with Thermal Analysis Controller. Retrieved from. https://www.ebay.com/i/233276027797?chn=ps&norover=1&mkevt=1&mkrid=711-117182-37290-0&mkcid=2&itemid=233276027797&targetid=475515141541&device=c&adtype=pla&googleloc=9005925&poi=&campaignid=1669934843&adgroupid=65058350579&rlsatarget=pla-475515141541&abcId=1139296&merchantid=8312934&gclid=EAIaIQobChMIt7uD_KSt4wIVG7jACh1IMQfHEAYYBSABEgKapfD_BwE.

Google, 2019. Prescale Pressure Sensitive Films. Retrieved from. https://www.google.com/search?q=prescale+pressure+sensitive+films&rlz=1C1GCEU_enUS843US843&source=lnms&tbm=shop&sa=X&ved=0ahUKEwj6vsDd6PjiAhVtzlkKHVfnBV8Q_AUIECgB&biw=1920&bih=969.

Google, 2019. Stylus Profilometer. Retrieved from. https://www.google.com/search?q=stylus+profilometer&rlz=1C1GCEU_enUS843US843&source=lnms&tbm=shop&sa=X&ved=0ahUKEwjT3eCE4PjiAhXLq1kKHVXZA6AQ_AUIECgB&biw=1920&bih=920.

Grönqvist, R., Roine, J., Järvinen, E., Korhonen, E., 1989. An apparatus and a method for determining the slip resistance of shoes and floors by simulation of human foot motions. Ergonomics 32 (8), 979–995.

Hemler, S., Beschorner, K.E., 2017. Effects of shoe wear on slipping – implications for shoe replacement threshold. In: Paper Presented at the Human Factors and Ergonomics Society, Austin, TX.

Imbimbo, M., De Luca, A., 1998. FE stress analysis of rubber bearings under axial loads. Comput. Struct. 68 (1), 31–39.

Iraqi, A., Cham, R., Redfern, M.S., Beschorner, K.E., 2018. Coefficient of friction testing parameters influence the prediction of human slips. Appl. Ergon. 70, 118–126. https://doi.org/10.1016/j.apergo.2018.02.017.

James, G., Witten, D., Hastie, T., Tibshirani, R., SpringerLink, 2013. An Introduction to Statistical Learning: with Applications in R, vol. 103. Springer, New York, NY (New York).

Jones, T., Iraqi, A., Beschorner, K., 2018. Performance testing of work shoes labeled as slip resistant. Appl. Ergon. 68, 304–312. https://doi.org/10.1016/j.apergo.2017.12.008.

Lindner, M., Sextro, W., Popp, K., 2004. Hysteretic friction of a sliding rubber element. In: Paper Presented at the PAMM: Proceedings in Applied Mathematics and Mechanics.

Lowe, B., Dempsey, P., Jones, E., 2018. Assessment methods used by certified ergonomics professionals. Proc. Hum. Factors Ergon. Soc. Annu. Meet. 62 (1), 838–842. https://doi.org/10.1177/1541931218621191.

Marucci-Wellman, H.R., Courtney, T.K., Corns, H.L., Sorock, G.S., Webster, B.S., Wasiak, R., Noy, Y.I., Matz, S., Leamon, T.B., 2015. The direct cost burden of 13 years of disabling workplace injuries in the US (1998–2010): findings from the Liberty Mutual Workplace Safety Index. J. Saf. Res. 55, 53–62.

Moghaddam, S.R.M., Acharya, A., Redfern, M.S., Beschorner, K.E., 2018. Predictive multiscale computational model of shoe-floor coefficient of friction. J. Biomech. 66, 145–152.

Moghaddam, S.R.M., Beschorner, K.E., 2017. Sensitivity of a multiscale model of shoe-floor-contaminant friction to normal force and shoe-floor contact angle. In: Paper Presented at the 2017 STLE Annual Meeting & Exhibition.

Moghaddam, S.R.M., Redfern, M.S., Beschorner, K.E., 2015. A microscopic finite element model of shoe–floor hysteresis and adhesion friction. Tribol. Lett. 59 (3), 42.

Neobits, 2019. Contact-angle meter. Retrieved from. https://www.neobits.com/cheminstruments_cam_plus_c_120_cheminstruments_cam_p9593509.html?atc=gbp&gclid=EAIaIQobChMIhKaP3OT44gIVg4rICh3LvgwtEAkYCCABEgJfj_D_BwE.

Nishi, T., Moriyasu, K., Harano, K., Nishiwaki, T., 2016. Influence of dewettability on rubber friction properties with different surface roughness under water/ethanol/glycerol lubricated conditions. Tribol. Online 11 (5), 601–607.

Perkins, P., Wilson, M., 1983. Slip resistance testing of shoes—new developments. Ergonomics 26 (1), 73–82.

Redfern, M.S., DiPasquale, J., 1997. Biomechanics of descending ramps. Gait Posture 6 (2), 119–125.

Shibata, K., Warita, I., Yamaguchi, T., Hinoshita, M., Sakauchi, K., Matsukawa, S., Hokkirigawa, K., 2019. Effect of groove width and depth and urethane coating on slip resistance of vinyl flooring sheet in glycerol solution. Tribol. Int. 135, 89–95.

Siegmund, G.P., Heiden, T.L., Sanderson, D.J., Inglis, J.T., Brault, J.R., 2006. The effect of subject awareness and prior slip experience on tribometer-based predictions of slip probability. Gait Posture 24 (1), 110–119.

Singh, G., Beschorner, K.E., 2014. A method for measuring fluid pressures in the shoe-floor-fluid interface: application to shoe tread evaluation. IIE Trans. Occup. Ergon. Human Factors 2 (2), 53–59.

Sridharan, K., Sivaramakrishnan, R., 2012. Dynamic behavior of tyre tread block. Am. J. Eng. Appl. Sci. 5 (2).

Strobel, C.M., Menezes, P.L., Lovell, M.R., Beschorner, K.E., 2012. Analysis of the contribution of adhesion and hysteresis to shoe–floor lubricated friction in the boundary lubrication regime. Tribol. Lett. 47 (3), 341–347.

Tencer, A.F., Koepsell, T.D., Wolf, M.E., Frankenfeld, C.L., Buchner, D.M., Kukull, W.A., Tautvydas, M., 2004. Biomechanical properties of shoes and risk of falls in older adults. J. Am. Geriatr. Soc. 52 (11), 1840–1846.

Tsai, Y.J., Powers, C.M., 2008. The influence of footwear sole hardness on slip initiation in young adults*. J. Forensic Sci. 53 (4), 884–888.

U.S. Department of Labor- Bureau of Labor Statistics, 2017. National Census of Fatal Occupational Injuires in 2016 (Washington, D.C).

U.S. Department of Labor- Bureau of Labor Statistics, 2018. Employer-reported Workplace Injuires and Illnesses – 2017 (Washington, D.C).

Verma, S.K., Chang, W.R., Courtney, T.K., Lombardi, D.A., Huang, Y.-H., Brennan, M.J., et al., 2011. A prospective study of floor surface, shoes, floor cleaning and slipping in US limited-service restaurant workers. Occup. Environ. Med. 68 (4), 279–285.

Wang, Y.-X., Ma, J.-H., Zhang, L.-Q., Wu, Y.-P., 2011. Revisiting the correlations between wet skid resistance and viscoelasticity of rubber composites via comparing carbon black and silica fillers. Polym. Test. 30 (5), 557–562.